Computational Science, Engineering and Technology Series: 30

Computational Methods for Engineering Science

Edited by
B.H.V. Topping

With contributions from: J.M. Adam, A. Ammar, J.V. Araújo dos Santos, R.C. Barros, K.J. Bathe, F. Bordeu, A. Borna, M.A. Bradford, P.A. Calderón, E. Carrera, E., M.B. Cesar, F. Chinesta, E. Cueto, R. Darvizeh, K. Davey, A. Eriksson, J. Garzón-Roca, W.G. Habashi, X. Jia, L. Kaczmarczyk, A.S.K. Kwan, A. Leygue, H. Lopes, F. Magoulès, H.A. Mang, K. Marti, G. McClure, M. Mousavi Nezhad, G. Muscolino, A. Pagani, F.J. Pallarés, C.J. Pearce, M. Petrolo, Y.-L. Pi, P.N. Psarropoulos, A. Sofi, Y. Tsompanakis and E. Zappino.

This volume includes the invited lectures presented at: *The Eleventh International Conference on Computational Structures Technology* and *The Eighth International Conference on Engineering Computational Technology* held concurrently in Dubrovnik, Croatia from 4-7 September 2012.

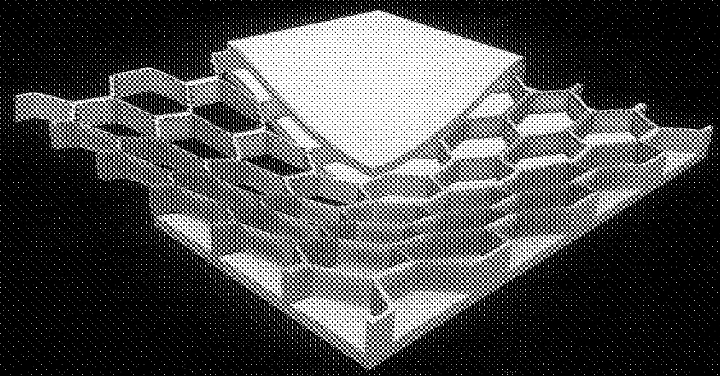

For further details of our computational technology books, see our website:
http://www.saxe-coburg.co.uk

SAXE-COBURG PUBLICATIONS CSETS: 30
ISSN 1759-3158 ISBN 978-1-874672-58-6

Computational Methods for Engineering Science
Edited by B.H.V. Topping

Computational Methods for Engineering Science

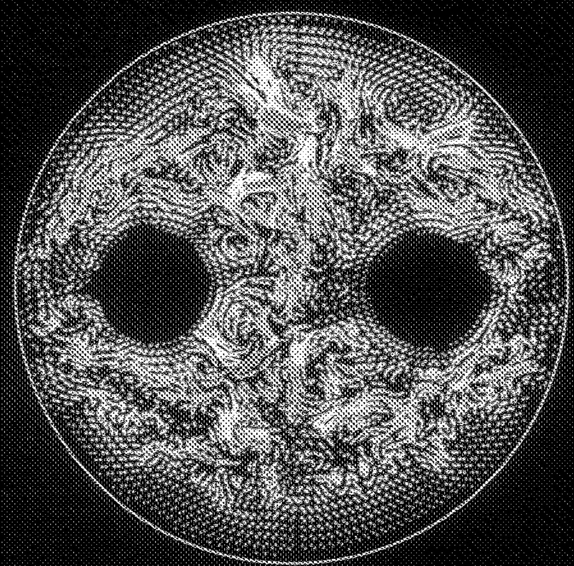

Edited by
B.H.V. Topping

SAXE-COBURG PUBLICATIO

Computational Science, Engineering and Technology Series: 30

Computational Methods
for
Engineering Science

Saxe-Coburg Publications on Computational Engineering

Soft Computing Methods for Civil and Structural Engineering
Edited by: Y. Tsompanakis and B.H.V. Topping

Civil and Structural Engineering Computational Technology
Edited by: B.H.V. Topping and Y. Tsompanakis

Trends in Parallel, Distributed and Grid Computing for Engineering
Edited by: P. Iványi and B.H.V. Topping

Developments and Applications in Engineering Computational Technology
Edited by: B.H.V. Topping, J.M. Adam, F.J. Pallarés, R. Bru and M.L. Romero

Developments and Applications in Computational Structures Technology
Edited by: B.H.V. Topping, J.M. Adam, F.J. Pallarés, R. Bru and M.L. Romero

Substructuring Techniques and Domain Decomposition Methods
Edited by: F. Magoulès

Soft Computing in Civil and Structural Engineering
Edited by: B.H.V. Topping and Y. Tsompanakis

Trends in Civil and Structural Engineering Computing
Edited by: B.H.V. Topping, L.F. Costa Neves and R.C. Barros

Parallel, Distributed and Grid Computing for Engineering
Edited by: B.H.V. Topping and P. Iványi

Trends in Computational Structures Technology
Edited by: B.H.V. Topping and M. Papadrakakis

Trends in Engineering Computational Technology
Edited by: M. Papadrakakis and B.H.V. Topping

Computational Methods for Acoustics Problems
Edited by: F. Magoulès

Mesh Partitioning Techniques and Domain Decomposition Methods
Edited by: F. Magoulès

Object Oriented Methods and Finite Element Analysis
R.I. Mackie

Programming Distributed Finite Element Analysis
R.I. Mackie

Computer Aided Design of Cable-Membrane Structures
B.H.V. Topping and P. Iványi

Computational Methods for Engineering Science

Edited by
B.H.V. Topping

SAXE-COBURG
PUBLICATIONS

© Saxe-Coburg Publications, Stirlingshire, Scotland

published 2012 by
Saxe-Coburg Publications
Dun Eaglais
Station Brae, Kippen
Stirlingshire, FK8 3DY, UK

Saxe-Coburg Publications is an imprint of Civil-Comp Ltd

Computational Science, Engineering and Technology Series: 30
ISSN 1759-3158
ISBN 978-1-874672-58-6

British Library Cataloguing in Publication Data
A catalogue record for this book is available from the British Library

Front cover image: Velocity vector plot of electromagnetic chaotic mixing in a channel, courtesy of ADINA. For more information, please refer to Chapter 1.
Back cover image: Analysis of the complex structure of a honeycomb plate. For more information, please refer to Chapter 10.

Printed in Great Britain by Bell & Bain Ltd, Glasgow

Contents

Preface

This volume comprises the Invited Lectures presented at *The Eleventh International Conference on Computational Structures Technology* (CST 2012) and *The Eighth International Conference on Engineering Computational Technology* (ECT 2012) held concurrently in Dubrovnik, Croatia from 4-7 September 2012. I am grateful to the authors and co-authors of the Invited Lectures included in this volume. Their contribution both to these conferences and to this book is greatly appreciated.

Other papers presented at this conference are published as follows:

- *The Invited Review Lectures from CST 2012 and ECT 2012 are published in:* Computational Technology Reviews, Volumes 5 and 6, Saxe-Coburg Publications, Stirlingshire, Scotland, 2012.
- *The Contributed Papers from CST 2012 are published in:* Proceedings of the Eleventh International Conference on Computational Structures Technology, B.H.V. Topping, (Editor), (Book of Summaries with online delivery of full-text papers), Civil-Comp Press, Stirlingshire, Scotland, 2012.
- *The Contributed Papers from ECT 2012 are published in:* Proceedings of the Eighth International Conference on Engineering Computational Technology, B.H.V. Topping, (Editor), (Book of Summaries with online delivery of full-text papers), Civil-Comp Press, Stirlingshire, Scotland, 2012.

I would like to thank the members of the CST 2012 and ECT 2012 Conference Editorial Boards for their help before and during the conference.

Finally, I am grateful to Jelle Muylle (Saxe-Coburg Publications) for his help in coordinating the publication of this book and for all his administrative and organisational skills in organising these conferences. I also wish to thank Dawn Sewell (Civil-Comp Press) for her administrative support.

UNIVERSITY OF PÉCS

HERIOT WATT UNIVERSITY

Professor B.H.V. Topping
University of Pécs, Hungary
& Heriot-Watt University, Edinburgh, UK

©Saxe-Coburg Publications, 2012.
Computational Methods for Engineering Science
B.H.V. Topping, (Editor)
Saxe-Coburg Publications, Stirlingshire, Scotland, 363-398.
doi:10.4203/csets.30.15

Chapter 15

Non-Linear and Hysteretic Analysis of the Behaviour of Magnetorheological Dampers

M.B. Cesar[1] and R.C. Barros[2]
[1]Department of Applied Mechanics
Polytechnic Institute of Bragança (IPB-ESTiG), Portugal
[2]Department of Civil Engineering
Faculty of Engineering of the University of Porto (FEUP), Portugal

Abstract

This chapter reviews the basic concept of MR fluids and provides an insight into the magnetorheological (MR) dampers non-linear behaviour through both experimental and numerical analyses. Several modelling techniques are available to represent the non-linear hysteretic behaviour of MR dampers. These models can characterize the performance of the MR device but they are usually dependent on experimental data that must be available to determine the parameters involved in the model formulation. Thus, in the present study a commercial MR damper was experimentally tested under several input excitations. Many parametric models are available in the literature with different levels of accuracy and complexity. After selecting some of the most common parametric numerical models, the related model parameters were obtained based on the measured responses and a comparison between the numerical and experimental results will be presented to validate the selected models.

Keywords: magnetorheological damper, hysteretic behaviour, Bouc-Wen model.

1 Introduction

The so-called "smart materials" have received the attention of researchers and engineers as a result of their ability to create smart devices that can be easily controlled by a small external perturbation, like temperature or a magnetic field. Some of the most promising smart devices are based on fluids with controllable properties like electrorheological (ER) and magnetorheological (MR) fluids.

The initial discovery and development of MR fluids is credited to Jacob Rabinow [1]. Originally, the research related to these fluids was focused on the ER fluid, however, in the last few years, MR fluids have been extensively studied as a result of their robustness for real-life engineering applications [2-4]. Basically, the main

aprovação na parte escolar.

differences between ER and MR are related to the operating temperature range, maximum yield stress, and their sensitivity to impurities.

The performance of MR fluids is less sensitive to temperature because the magnetic polarization mechanism remains unchanged over the operating temperature range and the MR fluids behaviour is not affected by impurities, which means that it is insensitive to contamination, while ER fluids are highly sensitive to moisture or impurities as a result of the manufacture and usage process.

MR fluids are non-Newtonian and rheologically stable suspensions with a shear yield strength, which can be controlled by a magnetic field. These fluids react promptly to the application of an external magnetic field (in a few milliseconds) exhibiting a reversible and adjustable transition from a free-flowing state to a semi-solid state. As a consequence of this property, these materials exhibit a significant change in their rheological behaviour (viscosity and plasticity).

Figure 1 illustrates the variation of the shear stress and apparent viscosity with shear strain for an MR fluid under different magnetic field strengths [5, 6]. In these plots it is possible to verify the characteristic MR fluid behaviour, especially the critical yield stress that defines the transition between pre-yield and post-yield regions and the apparent increase in viscosity.

The expression "apparent viscosity" is used because the carrier fluid viscosity does not change as the magnetic field intensity H is modified.

The rheological behaviour of MR fluids depends on the magnetic field strength H, however, it is possible to define pre and post yield areas as shown in Figure 1a. In the pre-yield region the MR fluid exhibits visco-elastic behaviour and in the post-yield region it behaves like a viscous Newtonian fluid.

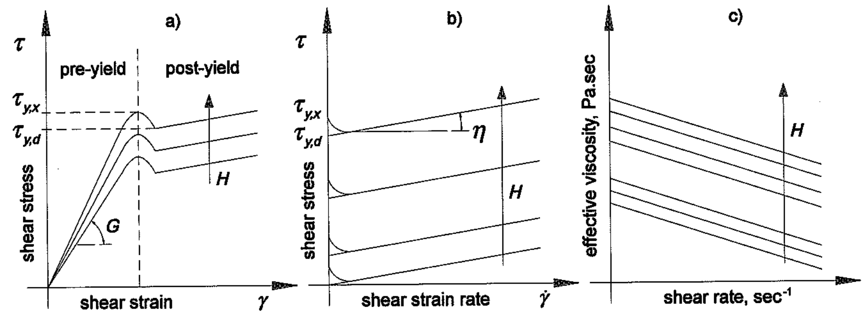

Figure 1: Constitutive behaviour of a MR fluid: a) pre-yield and post-yield regions, b) non-Newtonian post-yield behaviour and c) apparent viscosity

In can be stated that the transition from the pre-yield to the post-yield region occurs when the stress is greater than the yield shear stress. In this transition zone it is

possible to identify the dynamic shear yield stress $\tau_{y,d}$ defined as the point of the zero-rate, and the static shear yield stress $\tau_{y,s}$ defined as the shear stress necessary to initiate MR fluid flow [6, 7].

These are fundamental parameters that allow defining the characteristic shear stresses of the MR fluid.

2 Experimental response

The device employed in the testing, identification, and modelling of the non-linear hysteretic response is the RD-1005-3 commercial prototype developed by the LORD Corporation. Extensive experimental research was developed to evaluate and obtain the MR damper response data necessary to proceed with the identification procedure [8, 9]. The experimental tests were performed using an MTS universal testing machine load frame with an MTS load unit controller, as shown in Figure 2.

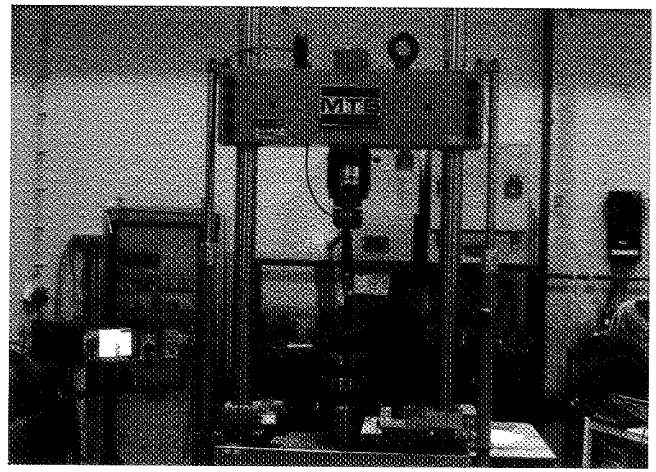

Figure 2: MTS universal testing equipment

In the MTS test machine, a hydraulic actuator is employed to drive the MR damper from sinusoidal displacement cycles with several amplitudes and frequencies. The MTS load frame is equipped with a displacement sensor to measure the displacement of the MR damper piston and a 5.0 kN load cell to measure the output force. A specific fixture was designed to attach the MR damper to the upper and lower heads of the load frame. The damper stroke was positioned at its center before starting the experimental program in order to avoid the extreme positions of the damper stroke. The signals of the piston displacement x and the output force f are sampled with a frequency rate of 1.0 kHz, while the piston velocity v is obtained from the derivative of displacement with respect to time.

The LORD MR damper is usually commanded through a voltage-to-current controller unit designated as a Wonder Box Device Controller and sold as a complementary product for MR devices. A representation of the Wonder Box device (with reference RD-3002-3) is shown in Figure 3 along with the voltage-to-current law of the device. The device provides a closed-loop current control to compensate for changing electrical loads up to the limits of the power supply and can be used to investigate the control possibilities of the LORD MR technology, since it can be operated as an interface device for PLC or the computer control of the MR fluid devices.

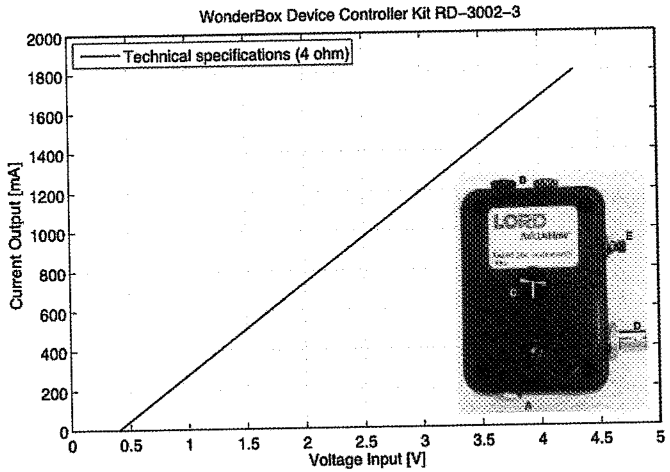

Figure 3: Wonder Box Device Controller RD-3002-3 from LORD Corp

The Wonder Box also allows a manual operation through a potentiometer in order to control the current supplied to the MR device. This controller was connected to a voltage power supply unit in order to feed the MR damper with a constant voltage converted to the current supply through the Wonder Box.

The RD-1005-3 MR damper shown in Figure 4 has a conventional cylindrical body configuration filled with 50 ml of MR fluid and comprising the piston, the magnetic circuit with a coil resistance of 5 Ω, and the accumulator. The enclosing cylinder is 41.4 mm in diameter and the damper is 208 mm long in its extended position with ±2.5 cm stroke.

The device can operate within a current range from 0.0 A up to 2.0 A with a recommended input value of 1.0 A for continuous operation, and can deliver a peak force of 2224 N at a velocity of 51 mm/s with a continuous operating current level of 1.0 A. The MR damper can reach at least 90% of maximum level during a 0.0 amp to 1.0 amp step input in less than 25 milliseconds.

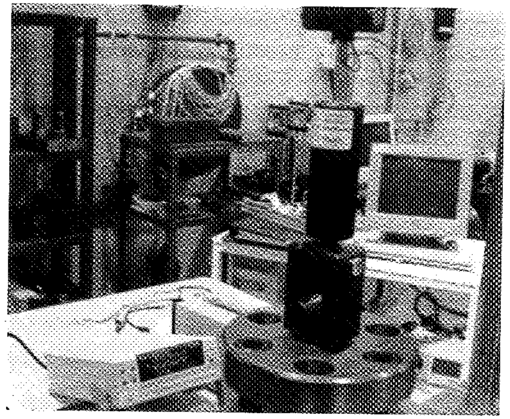

Figure 4: RD-1005-3 MR damper form Lord Corporation

A series of sinusoidal displacement excitation tests were performed to measure the response under different loading conditions in order to obtain the hysteretic response of the MR damper. The MR damper was mounted onto the MTS hydraulic actuation system and was then excited with a sinusoidal displacement. An extensive parametric study was carried out for several arrangements of amplitudes, frequencies, and input currents; these scenarios were studied in order to obtain the required experimental data to conveniently characterize the damper response [10, 11].

The selected parameters to develop the test program in order to determine the steady state characteristics of the damper for sinusoidal inputs comprise the set of frequencies, amplitudes, and current supplies specified in Table 1. To refine the experimental response of the MR damper, the applied current ranges from 0.0A to a maximum of 1.0A in increments of 0.25A. The input current range was refined from 0.0A to 0.25A to conveniently characterize the current dependent MR damper response at low current input.

Parameter	Values
Frequencies (Hz)	(0.50, 1.00, 1.50, 2.00)
Amplitudes (mm)	(2.0, 4.0, 6.0, 8.0, 10.0)
Current supplies (A)	(0.00, 0.10, 0.20, 0.25, 0.50, 0.75, 1.00)

Table 1: Parameter variation of the sinusoidal signal with several current supplies for the Lord RD-1005-3 MR damper experimental analysis

The testing procedure was carried out with a fixed frequency and amplitude sinusoidal displacement for a specific current supply, repeating this process for

every parameter combination. The experimental data from the parametric study for MR dampers are typically grouped according to the variability of the different parameters set as frequency-dependent tests and amplitude-dependent tests.
The sinusoidal shaft displacement and the resulting force are measured though the MTS internal LVDT and a force transducer (load cell) with a sampling rate of 256Hz, and logged for data analysis. The displacement and force transducers were calibrated previously to the experimental procedure to reduce measuring imprecisions. Based on the results, it is possible to generate the force-displacement (f-d) and force-velocity (f-v) hysteresis cycles of the damper and therefore understand and investigate the device rheological behaviour.

Figures 5 illustrates some of the experimental results obtained with the testing procedure. The plots were developed from the data records selecting an experimental response cycle for a steady state excitation.

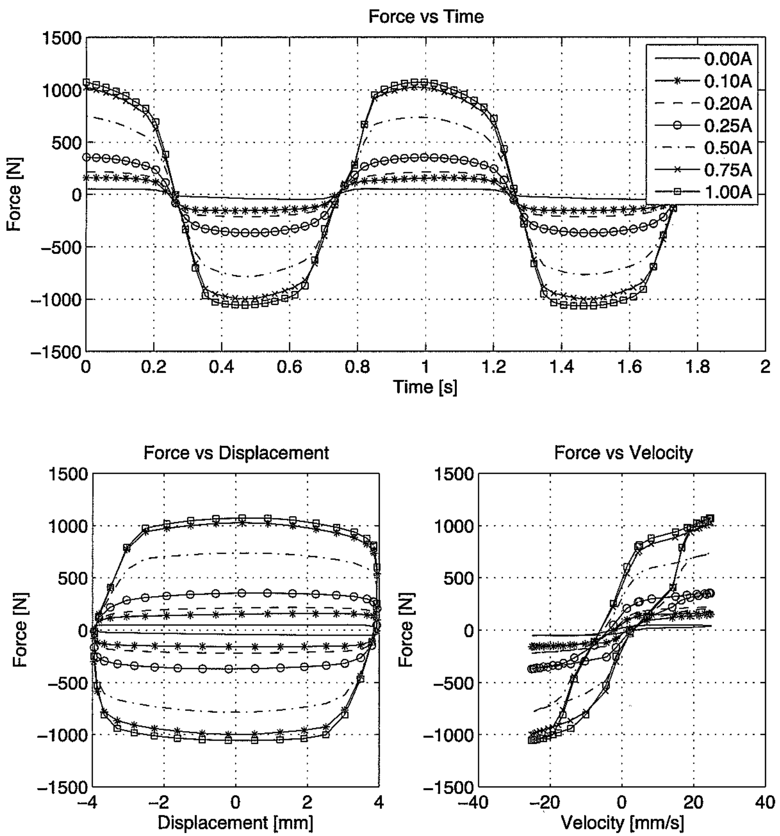

Figure 5: RD-1005-3 MR damper - Measured damping forces under a 1.00 Hz sinusoidal excitation with amplitude of 4.00 mm and variable input current

3 Numerical models

MR dampers are semi-active devices whose damping characteristics can be modified in real time as a result of their ability to adjust the resistance to flow of a MR fluid within the damper through the application of a magnetic field. The particular properties of the MR fluid allow variations in the damping force that can be controlled by varying an applied current. Thus, the hysteretic behaviour of an MR damper is current dependent, but also the function of the amplitude of the excitation. To predict the behaviour of MR dampers under certain magnetic fields or excitations, it is necessary to model the device with an appropriate approach. This becomes a relevant aspect because before producing an MR damper, it is necessary to design and select the correct parameters that will define the behaviour of the device.

Hence, a previous numerical simulation is needed to verify if the proposed properties are suitable for the system in which it is intended to apply the MR damper. Several numerical models are available to predict the response of MR dampers [12-16]. Table 2 presents a brief description of the available models for MR dampers.

The main problem regarding the modelling of MR dampers is related to the significant non-linear response that these devices exhibit when subjected to an input excitation. Moreover, the hysteretic behaviour observed is a function of the amplitude and frequency of excitation but (as a result of their rheological nature, and the semi-active controllable response) it is also current dependent, which considerably increases the difficulty level when a numerical model is developed. In order to use the MR damper as a controllable semi-active device in a control system, it is essential that the selected numerical model can capture its non-linear behaviour in order to develop a feasible semi-active controller [8-11].

Since many mathematical models have been developed to describe such behaviour, and to take advantage of the MR properties of these devices in vibration control related problems, it is necessary to select and implement high-accuracy models capable of capturing their non-linear hysteretic response. Among the modelling techniques, parametric models appear to be an easy and reliable approach to obtain a mathematical model of the physical MR damper.

Figure 6 illustrates the response of the Bingham, Bouc-Wen and Modified Bouc-Wen models [17-19], which are some of the most common models obtained by a deterministic approach.

Table 3 shows the different rheological components of these models, from which it is possible to verify that the very simple Bingham model has limited capabilities with which to model the MR damper behaviour, while the more elaborated modified Bouc-Wen model has the ability to include the hysteretic and the roll-off effect that is observed in most of the devices.

Modelling technique	MR damper Models
Bingham models	- Original Bingham model - Modified Bingham model - Gamota and Filisko model - Updated Bingham model by Occhiuzzi *et al.* - Three-element model by Powell
Bi-viscous models	- Nonlinear bi-viscous model - Nonlinear hysteretic bi-viscous model - Nonlinear hysteretic arctangent model - Lumped parameter bi-viscous model
Visco-elastic-plastic models	- General visco-elastic-plastic models - Visco-elastic-plastic model by Li *et al*
Stiffness-viscosity-elasto-slide model	- Stiffness-viscosity-elasto-slide (SVES) model
Hydro-mechanical model	- Hydro-mechanical model
Maxwell models	- BingMax model by Makris *et al.* - Maxwell Nonlinear Slider model
Bouc-Wen models	- Simple Bouc-Wen model - Modified Bouc-Wen model - Bouc-Wen model for shear mode dampers - Bouc-Wen model for large-scale dampers - Current dependent Bouc-Wen model - Current-frequency-amplitude dependent Bouc-Wen - Non-symmetrical Bouc-Wen model
Dahl models	- Modified Dahl model - Viscous Dahl model
LuGre models	- Modified LuGre model by Jimenez and Alvarez - Modified LuGre model by Sakai et al
Hyperbolic tangent models	- Hyperbolic tangent model by Kwok *et al*
Sigmoid models	- Sigmoid model by Wang *et al* and Ma *et al*
Equivalent models	- Equivalent model by Oh and Onoda
Phase transition models	- Phase transition model

Table 2: MR dampers Models classification

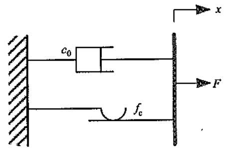

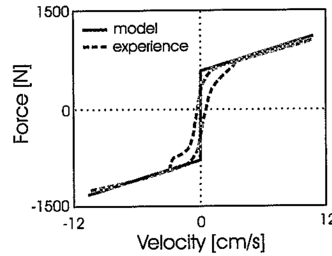

a) $F(t) = c_0\dot{x} + f_c\,\mathrm{sgn}(\dot{x}) + f_0$

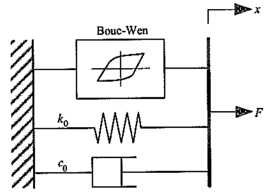

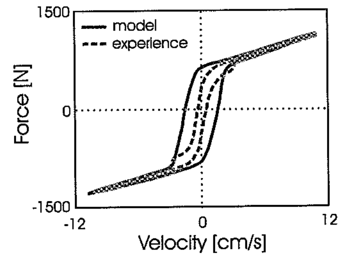

b) $F(t) = c_0\dot{x} + k_0(x - x_0) + \alpha z$

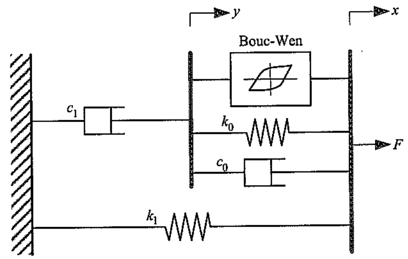

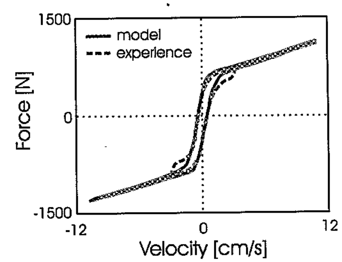

c) $F(t) = c_1\dot{y} + k_1(x - x_0)$

Figure 6: MR-fluid and MR-dampers models [17, 18] a) Bingham model, b) Bouc-Wen model, c) Modified Bouc-Wen model

MR damper model	MR damper behaviour				
	viscotic	elastic	plastic	hysteretic	Roll-off
Bingham	✓		✓		
Bouc-Wen	✓	✓		✓	
Modified Bouc-Wen	✓	✓		✓	✓

Table 3: Rheological components of the most common parametric models

The Bingham mechanical model consists of a Coulomb friction element placed in parallel with a viscous damper and comprises the identification of three parameters (Figure 6): the frictional force f_c, the viscous damping parameter c_0, and the force as a consequence of the presence of the accumulator f_0.

The simple Bouc-Wen model presents a highly effective model for hysteretic systems and has become one of the most common approaches to describe the hysteretic behaviour of MR dampers. The force generated by the MR damper can be expressed by the combination of three elements (Figure 6): a dashpot defined by the damping coefficient c_0, a linear spring defined by the parameter k_0, and a Bouc-Wen component defined by the Bouc-Wen parameter α that represent the stiffness for the damping force component (yield stress of the MR fluid) associated with the evolutionary variable z that accounts for the history dependence of the response.

The non-linear hysteretic behaviour of the device is controlled by the Bouc-Wen component that is related to the restoring force of a non-linear hysteretic system as proposed by [20]. According to the Bouc-Wen formulation, the restoring force of the nonlinear hysteretic system $Q(x,\dot{x})$ can be decomposed into two parts as

$$Q(x,\dot{x}) = g(x,\dot{x}) + z(x) \tag{1}$$

where $g(x,\dot{x})$ is a non-hysteretic component expressed by the displacement x and velocity $\dot{x}$, while $z(x)$ is a hysteretic component defined by the displacement and the evolutionary variable z given by

$$\begin{aligned} \dot{z} &= -\beta\left|\dot{x}\right|z^{n} - \gamma\dot{x}\left|z\right|^{n} + A\,\dot{x}, \qquad & n &= 1,3,5,\ldots \\ \dot{z} &= -\beta\left|\dot{x}\right|z^{n-1} - \gamma\dot{x}\,z^{n} + A\,\dot{x}, \qquad & n &= 2,4,6,\ldots \end{aligned} \tag{2}$$

These equations are implemented in the simple Bouc-Wen model with an equivalent formulation in which the evolutionary variable is written as

$$\dot{z}(t) = -\beta\left|\dot{x}(t)\right|z(t)\left|z(t)\right|^{n-1} - \gamma\dot{x}(t)\left|z(t)\right|^{n} + A\,\dot{x}(t) \tag{3}$$

The evolutionary variable equation depends on four parameters A, β, γ, and n that represent the linearity in the unloading region and the smoothness of the transition from the pre-yield to post-yield regions.

Parameters A, β, and γ describe the shape and size of the hysteresis loop, and the parameter n controls the smoothness of the transition from elastic to plastic response. To avoid numerical errors when $0< n <1$, the evolutionary variable equation can be rewritten in the following form

$$\dot{z}(t) = \dot{x}(t)\left\{A - \left[\gamma + \beta\,\mathrm{sgn}(\dot{x}(t)\,\mathrm{sgn}(z(t)))\right]\left|z(t)\right|^{n}\right\} \tag{4}$$

that can be derived as

$$\frac{dz}{dx} = A - \left[\gamma + \beta\,\mathrm{sgn}(\dot{x}(t)\,\mathrm{sgn}(z(t)))\right]\left|z(t)\right|^{n} \tag{5}$$

and the ultimate value of z can be computed by setting $dz/dx = 0$ and is given by

$$z_{\max} = \left[\frac{A}{\beta+\gamma}\right]^{\frac{1}{n}} \tag{6}$$

It can be stated that setting the non-hysteretic component $g(x,\dot{x})$=0 the restoring force will become $Q(x,\dot{x})$=$z(x)$. Then, if z=0, dQ/dx= dz/dx =A, and hysteretic curves for different excitation and response levels will have the same slope when Q=$Q(z)$ and the loading and unloading path are identical [20]. Thus, the non-hysteretic term must be used to overcome inconsistencies between the numerical model and the experimental results. The force generated by the MR damper can be expressed by the four parameters (A, β, γ, and n) and a combination of the three parameters c_0, k_0, and α related to the physical components of the model.

The variable x_0 that appears in the Bouc-Wen model represents the initial displacement of the linear spring and is related to the force offset during the experimental tests.

The evolutionary variable equation contains four parameters that have a strong effect on the hysteresis response curve.

Thus, it becomes very important to study the influence of each parameter on the hysteresis development, mainly to define some initial values or constraints in order to reduce the complexity (the number of variables) of the identification procedure.

A comprehensive analysis of the influence of the Bouc-Wen parameters on the hysteretic behaviour of this model has been addressed in some previous research programs [21-23]. Hereafter, an analogous methodology will be used in the present section to study the influence of the model parameters in the hysteretic loops for a steady-state response in order to select the appropriate set of parameters that will match the experimental results.

According to the Bouc-Wen formulation, the shape of the hysteretic loop is defined by parameters A, β, γ, and n. Parameters A, β, and n are positive real numbers, while γ can be a positive or negative real number. The following study will be carried out for a harmonic periodic excitation x= x_0 sin(w(t)), where w= 1rad/s is the frequency and x_0 the amplitude of excitation.

The parameter A defines the scale and amplitude of the hysteresis loop and also controls the slope of the hysteresis loop at z=0 (the stiffness characteristic) as shown in Figure 7. In this plot, the parameters β and γ were kept constant (β= 0.5 and γ= -0.4) and the parametric variation of A for a fixed value of n= 1.0 was carried out. Increasing the parameter A will generate a larger hysteresis loop (with an increase in the curve slope) that implies an increase in the energy dissipation.

The parameter n is related to the smoothness of the transition from the linear to the non-linear region.

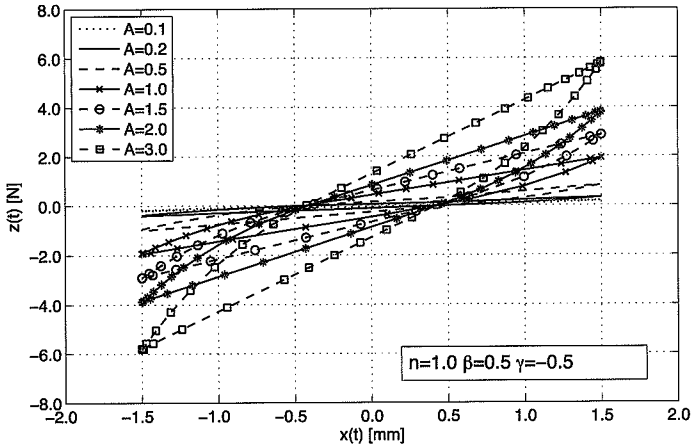

Figure 7: Influence of parameter A on the hysteretic behaviour

The influence of this parameter in the hysteresis loop is shown in Figure 8. In this case, parameters β, γ, and A are constant (β= 0.5, γ= -0.4 and A= 1.0) while the parameter n is changed.

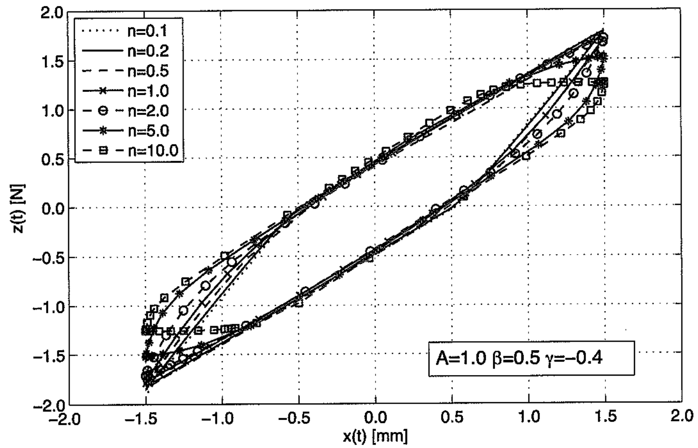

Figure 8: Influence of parameter n on the hysteretic behaviour

The parametric studies show that this power parameter n has a significant effect on the hysteresis loop when $1 < n < 2$ and practically no effect when $n > 2$.

Thus, the parameter n is usually set to n= 2. Moreover, increasing the value of parameter n will produce an elasto-plastic behaviour and for n=∞, the system will exhibit a true elasto-plastic behaviour [10].

The parameters β and γ are related to the shape of the hysteresis curve and different combinations of these parameters will describe several hysteretic loops with variations in the stiffness characteristics.

The slope dz/dx of the hysteresis curve in the loading and unloading cases can be used to study the influence of these parameters on the hysteretic behaviour. Table 4 shows the behaviour of the slope of the hysteresis loop.

dz/dx	$z > 0$	$z = 0$	$z < 0$
$\dot{x} > 0$	$A-(\gamma+\beta)\lvert z\rvert^n$	A	$A-(\gamma-\beta)\lvert z\rvert^n$
$\dot{x} > 0$	$A-(\gamma-\beta)\lvert z\rvert^n$	A	$A-(\gamma+\beta)\lvert z\rvert^n$

Table 4: Slope of the hysteresis loop [10]

The dependence of the hysteretic loops on the parameter β is shown in Figure 9 for A=1, γ=0.9 and n=1. Essentially, the parameter β controls the variation in the stiffness when the sign of the velocity variable changes.

Hence, the response exhibits a linear hysteretic behaviour when β=0, a hardening hysteretic behaviour when β<0 and a softening hysteretic behaviour when β>0.

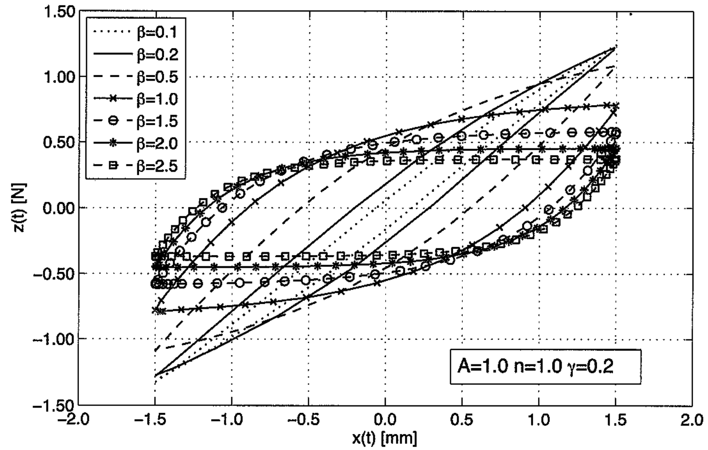

Figure 9: Influence of parameters β on force-displacement curves

The parameter γ is related to the area and flatness of the hysteresis loop as shown in Figure 10. Increasing the value of γ will produce a decrease in the loop inclination producing a flat hysteretic curve with a near horizontal branch. Also, when the parameter is below a certain value defined as γ_0 the area will increase.

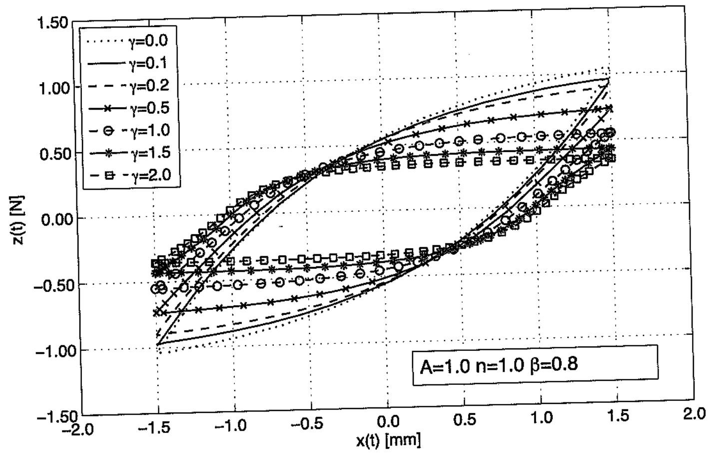

Figure 10: Influence of parameter γ on the hysteretic behaviour

However, when γ is larger than γ_0, the hysteretic loop becomes almost horizontal and the area slightly decreases, *i.e.*, the energy dissipated per cycle decreases. The parameters β and γ are related to the shape of the hysteresis curve and different combinations of these parameters will describe several hysteretic loops.

Therefore, it is important to study the relationship between these parameters to understand the influence of each combination in the hysteretic shape. The influence of the combination of these parameters in the hysteretic behaviour can be studied investigating the slope dz/dx of the hysteresis curve under loading and unloading.

When the loop is loading, the model shows a softening non-linear behaviour that occurs as a result of the fact that the slope of the hysteresis curve for z>0 decreases with the increase of z when $(\beta+\gamma)>0$ displaying a softening effect. The model exhibits hardening non-linearity produced by the increase in the slope of the hysteresis curve for $z>0$ with the increase of z when $(\beta+\gamma)<0$. Finally, the slope during loading for $z>0$ is kept constant and the system behaves quasi-linearly when $(\beta+\gamma)=0$. On the other hand, when the loop is unloading, the slope of the hysteresis curve for z> 0 decreases with the decrease of z when $(\beta-\gamma)>0$, increases with the decrease of z when $(\beta-\gamma)<0$ and is kept constant when $(\beta-\gamma)=0$ [11]. Eight possible combinations of β and γ can be used, however, only five of these combinations define hysteresis curves (or cases) that have physical meaning. The other three combinations are possible but these will not lead to a hysteretic behaviour and consequently they are not considered further. The possible combination of β and γ are summarized in Table 5.

Case	**Combinations**	**Hysteretic response**
I	$(\beta+\gamma)>0$ and $(\beta-\gamma)>0$	Softening non-linear behaviour during loading due to $(\beta+\gamma)>0$
II	$(\beta+\gamma)>0$ and $(\beta-\gamma)<0$	
III	$(\beta+\gamma)>0$ and $(\beta-\gamma)=0$	
IV	$(\beta+\gamma)<0$ and $(\beta-\gamma)>0$	Hardening non-linear behaviour during loading due to $(\beta+\gamma)<0$
V	$(\beta+\gamma)=0$ and $(\beta-\gamma)>0$	Quasi-linear behaviour during loading due to $(\beta+\gamma)=0$
Others	$(\beta+\gamma)=0$ and $(\beta-\gamma)<0$ $(\beta+\gamma)<0$ and $(\beta-\gamma)<0$ $(\beta+\gamma)<0$ and $(\beta-\gamma)=0$	Combinations without physical meaning

Table 5: Hysteretic response produced by β and γ combinations

A parametric study for each case and the corresponding hysteresis loops are shown in Figure 11 [10], [11]. The parameters A and n were both kept constant at 1.0 and the arrow indicates the loading to unloading direction. In the first three cases it is visible as a softening non-linear behaviour during loading as a result of a decrease of the loop slope produced by an increase of z (for positive values of z) when $(\beta+\gamma)>0$. In the fourth case, the system reveals a hardening non-linearity during loading as a result of an increase of the loop slope produced by an increase of z (with $z>0$) when $(\beta+\gamma)<0$.

In the fifth and final case with physical meaning, the slope during loading for $z>0$ remains constant and the system presents a quasi-linear behaviour when $(\beta+\gamma)=0$.

As expected, when the curve is in the unloading path, the slope for $z>0$ decreases with the decrease of z when $(\beta-\gamma)>0$, increases with the decrease of z when $(\beta-\gamma)<0$ and remain constant when $(\beta-\gamma)=0$. The hysteretic curves in Figures 11a and 11c have a similar shape and amplitude, which suggests that different combinations of β and γ can produce the same hysteretic response. Thus the use of the two parameters can be redundant and the combination of β and γ can be replaced by a single parameter β.

Figure 12 shows the hysteretic loops for two combinations of β and γ (β=0.8, γ=0.2 and $\beta=\gamma=0.5$) to demonstrate that different combinations of these parameters can generate the same hysteretic behaviour. In these combinations $(\beta+\gamma)=1$ and although a slight difference in the hysteresis amplitude is present arising from a larger value of β in the first combination, the hysteretic response in both cases is almost identical, and by adjusting the value of each parameter it is possible to obtain equivalent curves.

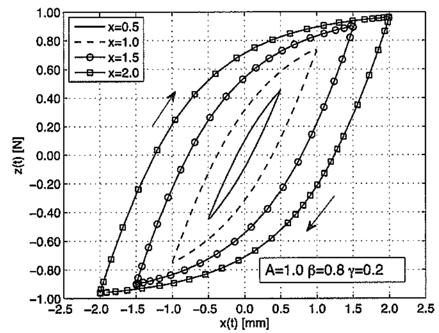

a) $(\beta+\gamma)>0$ and $(\beta-\gamma)>0$

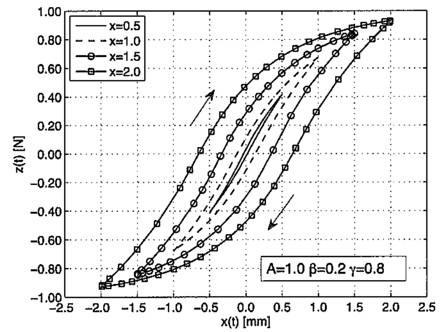

b) $(\beta+\gamma)>0$ and $(\beta-\gamma)<0$

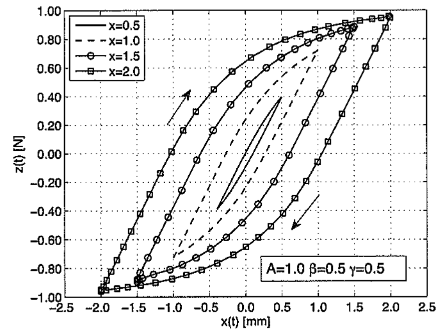

c) $(\beta+\gamma)>0$ and $(\beta-\gamma)=0$

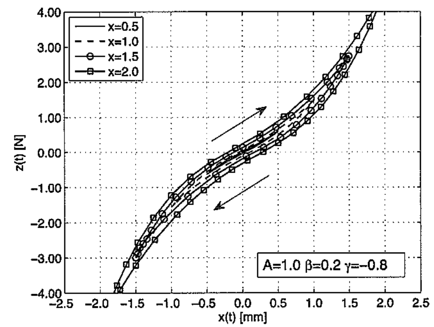

d) $(\beta+\gamma)<0$ and $(\beta-\gamma)>0$

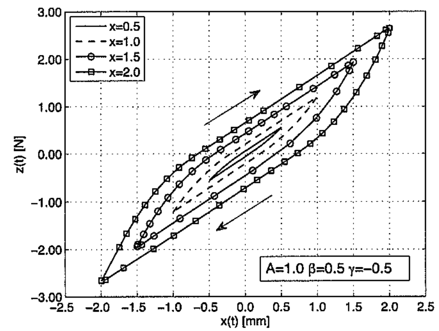

e) $(\beta+\gamma)=0$ and $(\beta-\gamma)>0$

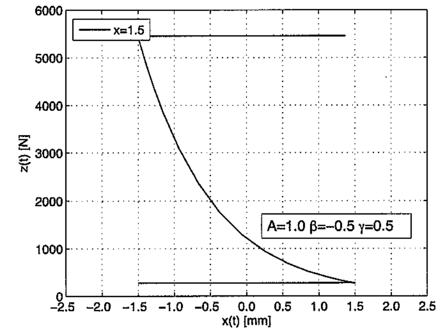

f) Other $(\beta+\gamma)=0$ and $(\beta-\gamma)<0$

Figure 11: Hysteresis loops for several combinations of β and γ

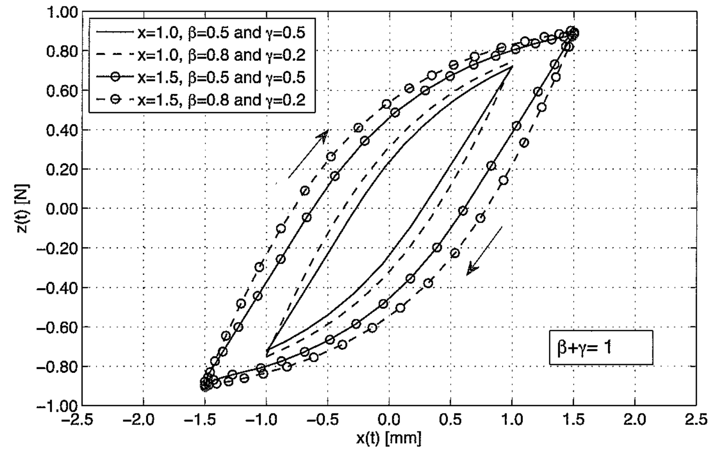

Figure 12: Hysteresis loops for two combinations of β and γ. Comb1 (β= 0.8, γ= 0.2) and Comb2 (β= 0.5, γ= 0.5)

Therefore it is possible to justify the use of the following relationship

$$\beta+\gamma=\text{constant} \qquad (7)$$

as also controlling parametric studies or defining the range of the parameters variation.

The relevance of the softening or hardening effect is determined by the combination of these parameters. Observing the third hysteretic curve, the system exhibits softening hysteretic behaviour since ($\beta+\gamma$)>0. Besides, in this case β=γ=0.5 and, consequently, the parameter γ can be neglected in the Bouc-Wen model, leading to a simpler identification procedure.

Finally, a brief reference regarding the rest of the Bouc-Wen parameters (c_0, k_0, and α) will be made.

These parameters are related to the three physical components of the model and they essentially affect the height of the global hysteretic loop and the slope and width of the hysteresis "tails", *i.e.*, the shape of the extension branch of the hysteretic curve. Essentially, the parameter α is a scale factor and the parameters c_0 and k_0 are related to the representation of a conventional damper behaviour.

Figure 13 shows the influence of the parameter α in the global hysteretic loop (since this parameter is a multiplier of the evolutionary variable z). In this case, the parameter α is increased from 10N to 60N with increments of 10N while the other parameters are kept constant (A= 20.0, β=γ= 5.0, n= 2.0 and c_0= k_0= 0.0).

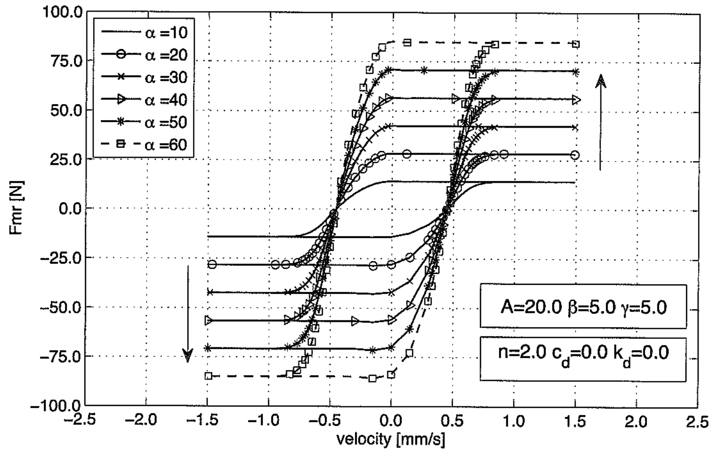

Figure 13: Influence of parameter α on force-velocity curves

According to the resulting plot, it is possible to verify that increasing the value of α will increase the height of the hysteresis loop. Thus, this parameter is responsible for the amplification of the vertical scale of the Bouc-Wen curve and can be seen as a scale factor of the hysteresis loop.

The parameter c_0 is a damping constant in the Bouc-Wen model that represents the post-yield relationship between the damper force and the velocity and generates an inclined line with a slope defined by the parameter value. This parameter essentially controls the slope of the hysteresis loop's external branches.

The effect of c_0 in the hysteresis loop is shown in Figure 14 for constant values of A= 20.0, β=γ= 5.0, n= 2.0, α= 30 and k_0= 0.0.

Changing the parameter causes a variation of the hysteresis loop slope with particular incidence in the external branch of the loop. Then, increasing the damping coefficient causes a rising in the slope of the hysteresis tails and large values of c_0 provide a steep inclination.

Finally, the effect of the spring parameter k_0 in the hysteresis loop is studied.

This parameter represents a stiffness parameter that generates a horizontal ellipse and is responsible for widening the ellipse shape around the zero velocity area.

Figure 15 represents the influence of this parameter in the global hysteresis shape when A= 20.0, β=γ= 5.0, n= 2.0, α= 30 and c_0= 10.0. When the coefficient k_0 is increased, the spring component of the Bouc-Wen model will become more significant producing an enlargement of the area enclosed in the hysteresis loop (a wider ellipse). It is also observed that large values of k_0 will produce a significant widening effect on the post-yield hysteresis ends instead of the pre-yield region.

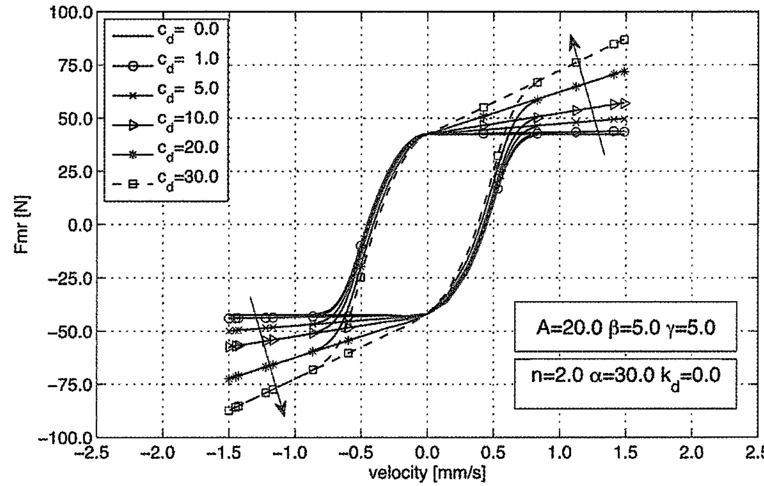

Figure 14: Influence of parameter c_0 on force-velocity curves

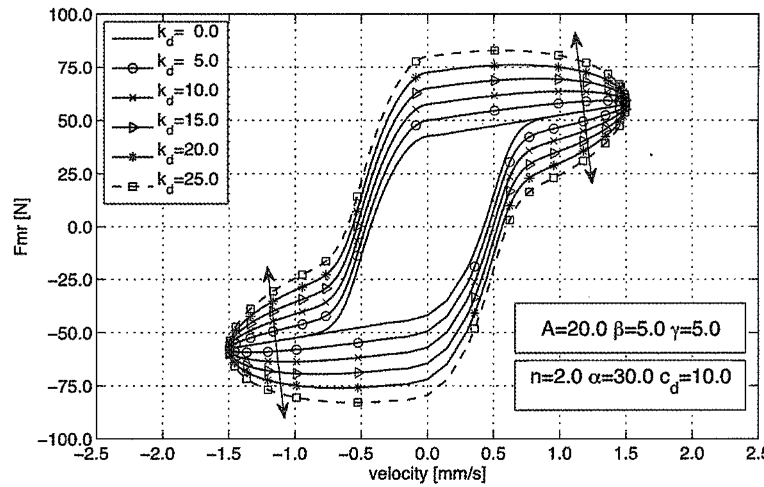

Figure 15: Influence of parameter k_0 on force-velocity curves

4 Parameters identification

High-accuracy models usually comprise a large number of parameters that require a reliable parameter identification procedure to efficiently estimate the suitable model parameters and reduce large parameter identification errors. Thus, the parameter identification methodology has a meaningful function in the development of a control problem and a large number of methodologies have been suggested and developed to solve this issue. This issue was addressed in the preceding section where the model formulation, the number of parameters associated with each parametric model, and the various identification possibilities were presented.

Usually, the parameter identification approach consists of formulating an optimization problem to find the best match between the experimental data and the dynamic model representation. To implement the identification procedure, the parameters can be defined as a vector of coefficients Θ that must be identified as

$$\Theta = [\Theta_1, \ldots, \Theta_n] \tag{8}$$

To compare the experimental response with the model-predicted response, the following performance criterion or objective function J can then be introduced

$$J(\Theta) = F_{mr}(\Theta) - F_e \tag{9}$$

where F_{mr} is the model-predicted force and F_e is the force obtained in the experimental procedure. Finally, an optimization algorithm can be used to adjust model parameters in order to minimize the objective function

$$\min_{\Theta} \sum_{i}^{N} J(\Theta)^2 = \min_{\Theta} \sum_{i}^{N} (F_{mr}(\Theta) - F_e)^2 \tag{10}$$

where N is the number of points in the experimental data or experimental samples.

The estimation of the model parameters can be established based on several numerical approaches such as least square methods, fuzzy methods, neural networks, genetic algorithm, *etc.* The least square method is a simple and standard approach to reduce the difference between an experimental value and the fitted value provided by a dynamic model, and the application of this method is mostly appropriate for models that have linear variations in the parameters.

However, the dynamic models for MR dampers are nonlinear in the parameters and a nonlinear approach should be considered to estimate model parameters. Nonlinear least squares regression generalizes and extends the linear least squares regression model to a much larger and more general class of functions, especially functions that cannot be linearized, and it is often used to identify the non-linear parameters of the numerical models of MR dampers. Although the linear and non-linear least square regression theoretically uses the same procedure to estimate the unknown parameters, there are very few limitations on the way parameters can be used in the functional part of a nonlinear regression model (when compared with the linear regression).

Therefore, the non-linear least square regression model will be used in the present study to estimate the model parameters for several numerical models.

There are several computational routines to solve nonlinear curve-fitting (data-fitting) problems such as *lsqnonlin* and *lsqcurvefit* routines in the MATLAB Optimization Toolbox [24]. *Lsqnonlin* routine solves nonlinear least squares

problems, including nonlinear data fitting problems, and *lsqcurvefit* is used to solve nonlinear curve fitting (data fitting) problems in the least squares sense. Both routines use the same algorithm and the *lsqcurvefit* routine is implemented to provide an interface designed specifically for data fitting problems. In this study both routines were used, although *lsqcurvefit* routine was used as the main least-square solver because it provides a convenient interface for data-fitting problems. The routine find coefficients x (related with Θ) that solve the problem

$$\min_{\Theta} \sum_{i}^{N} (F(x, xdata_i) - ydata_i)^2 = \min_{\Theta} \sum_{i}^{N} (F_{mr,i}(\Theta) - F_{c,i})^2 \tag{11}$$

given input data *xdata,* and the observed output *ydata*, where *xdata* and *ydata* are matrices or vectors, and F (x, *xdata*) is a matrix-valued or vector-valued function of the same size as *ydata.*

After defining the identification procedure, it is necessary to select the main numerical models that will be considered to simulate the MR damper response. In this case, the Bingham model, the simple Bouc-Wen, and the Modified Bouc-Wen model will be used for the RD-1005-3 MR damper

4.1 Bingham model

The Bingham model involves the identification of three parameters (f_c, c_0, and f_0). Therefore, the identification procedure is related to an optimization problem involving the parameter vector

$$\Theta = [f_c, c_0, f_0] \tag{12}$$

The force arising from the accumulator can be determined directly from the experimental response since the accumulator produces a nearly constant force offset (f_0 =40N) that can be measured by centering the experimental response plot. The parameters f_c and c_0 are voltage/current dependent and their values were computed with the parameter identification procedure previously described.

Figure 16 and 17 show the results that were obtained with the parameter identification procedure for the Bingham model when the damper is driven with a harmonic excitation of 1.50 Hz with 4 mm amplitude and an operating current of 0.25 A and 0.75 A, respectively.

This procedure was carried out for each set of experimental tests and the values of the mechanical parameters f_c and c_0 of the Bingham model were determined. Then, a polynomial curve fitting was used to find the functions that will relate to the mechanical model parameters with the operating current.

In this case, a third order polynomial function was chosen for the parameter f_c shown in Figure 18. Thus, the polynomial function that defines the parameter f_c is given by

$$f_c(I) = -910.09I^3 + 986.49I^2 + 663.56I + 52.19 \text{ (N)} \tag{13}$$

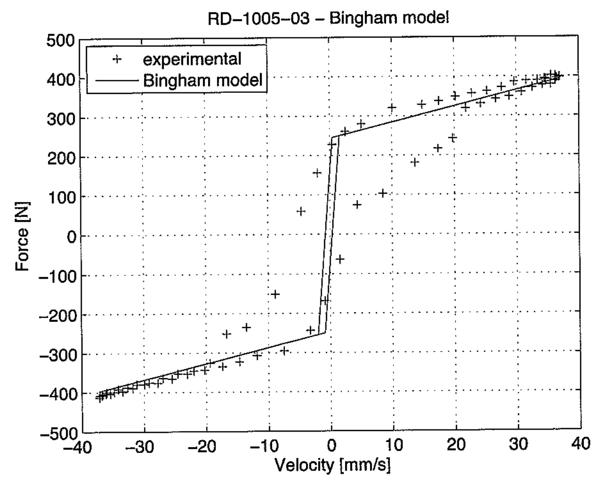

Figure 16: RD-1005-3 MR damper – Parameter identification of the Bingham model under a 1.50 Hz sinusoidal excitation with 4 mm amplitude and 0.25 A

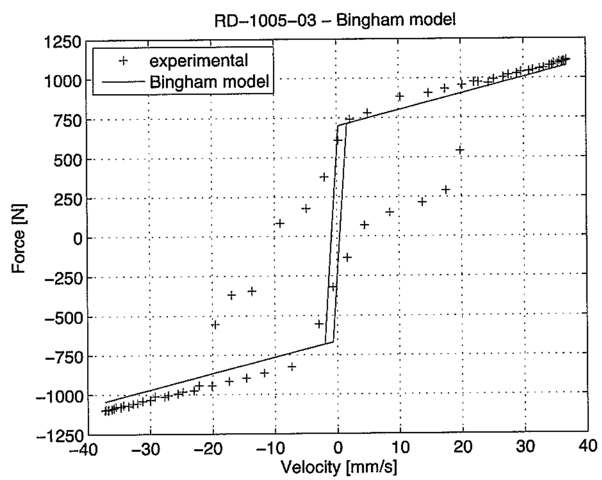

Figure 17: RD-1005-3 MR damper – Parameter identification of the Bingham model under a 1.50 Hz sinusoidal excitation with 4 mm amplitude and 0.75 A

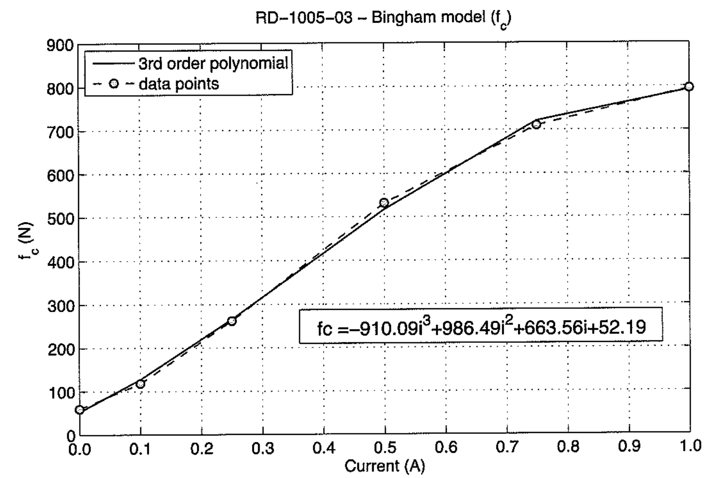

Figure 18: Curve fitting for $f_c(I)$ of the Bingham model

The model parameter c_0 shown in Figure 19 is given by the fourth polynomial function

$$c_0(I) = 48.74I^4 - 106.39I^3 + 66.00I^2 + 1.43I + 0.53 \text{ (N.s/mm)} \tag{14}$$

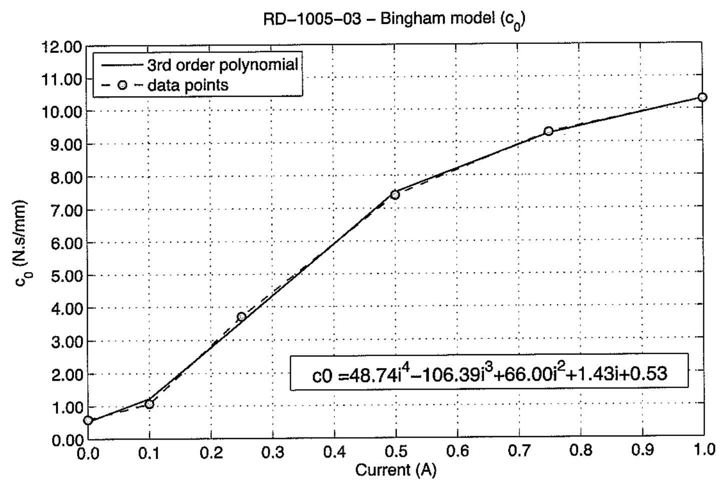

Figure 19: Curve fitting for $c_0(I)$ of the Bingham model

Figure 20 shows the comparison between the experimental data and the numerical curves for a 1.5 Hz sinusoidal excitation with 4 mm of amplitude and an operating current of I=1.00 A.

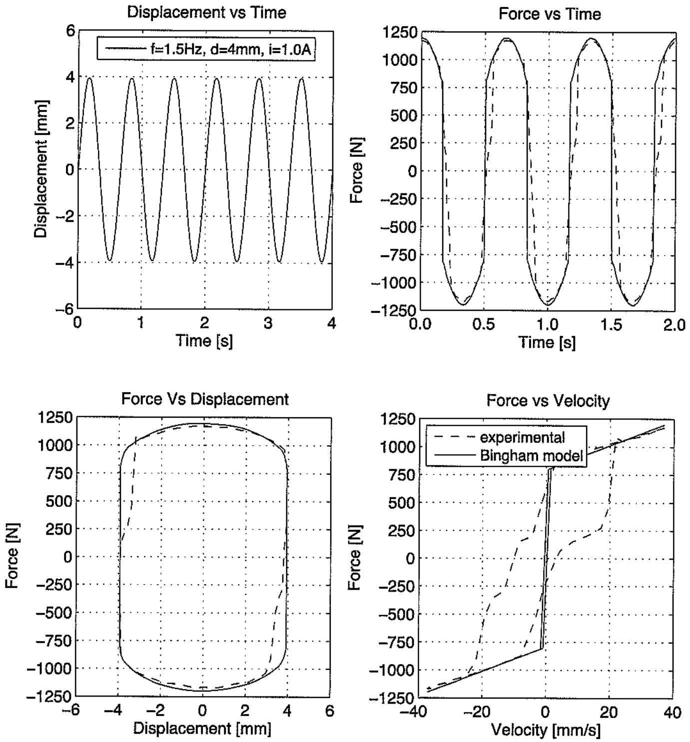

Figure 20: RD-1005-3 MR damper – Experimental vs. numerical response Bingham model (1.50 Hz sinusoidal excitation with 4mm amplitude and 1.00A)

As expected, the Bingham model can generally simulate the general pattern of the response of the MR damper, but not its very specific details. In fact, as a consequence of its simple rheological modelling capabilities, the model is unable to capture the hysteretic behaviour and the numerical results do not accurately fit the experimental data.

4.2 Simple Bouc-Wen model

Each numerical hysteretic loop is determined by a set of model parameters using the identification routine in order to match as closely as possible the experimental data. The first step of this identification procedure comprises the selection of the appropriate constraints associated with each parameter to reduce the complexity of the system. According with the experimental data, the damper has a softening

hysteretic effect with no signs of hardening, which indicates that parameters β and γ are in case I, II or III, *i.e.*, $(\beta+\gamma)>0$.

Likewise, the parameters A, α, k_0, and c_0 are positive variables. The experimental results show that the two ends of the hysteresis loops have a linear form with a moderate slope and with almost no widening effect.

Then, c_0 should have a reduced value to avoid steep slopes, and k_0 should be close to zero to reduce the widening effect.

It was assumed that n=2 since previous research suggests that this value provides an adequate matching between the model parameters and the experimental data. The force offset f_0 =40N has the same value as the Bingham model force offset.

Figure 21 shows the results that were obtained with the parameter identification procedure for the Bouc-Wen model when the damper is driven with a harmonic excitation of 1.50 Hz with 4mm amplitude and an operating current of 0.75A.

The identification procedure was carried out for each set of experimental data and the values of the model parameters of the Bouc-Wen model were determined.

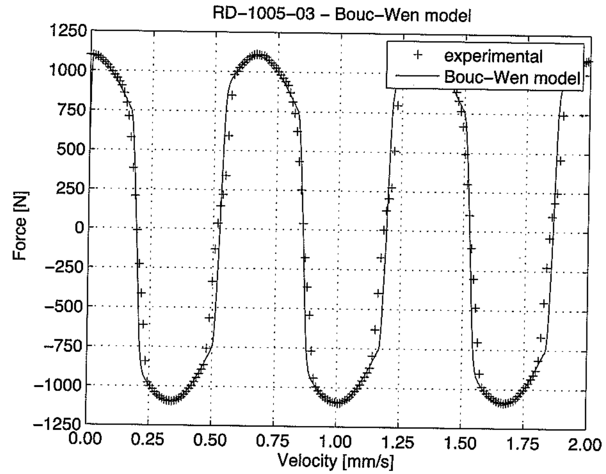

Figure 21: RD-1005-3 MR damper – Parameter identification of the Bouc-Wen model under a 1.50 Hz sinusoidal excitation with 4mm amplitude and 0.75A

It was observed that parameters A, β, γ show slow change with frequency, amplitude, and input current. Thus, these parameters can be classified as current/voltage independent, and they can be considered as constant values in the parametric model. In this case, the average values of the current independent parameters A=30.852, β=0.081 mm^{-2}, γ=1.507 mm^{-2} and k_0 =1.984 N/mm were found.

On the other hand, the parameters α and c_0 are current/voltage dependent and they can be described as functions of the input current or voltage delivered to the MR damper. Figures 22 and 23 show the variations of the model parameters α and c_0 with respect to the delivered current. As in the previous approach, the average values of each set of frequencies and amplitudes for a specific operating current were used to define the points displayed in these figures.

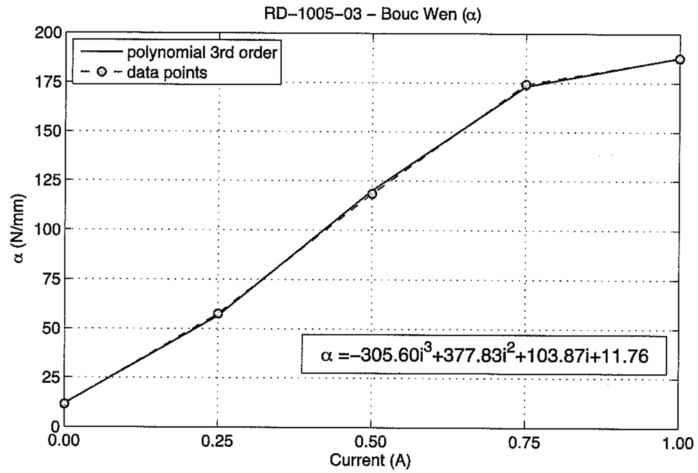

Figure 22: Curve fitting for $\alpha(I)$ of the Bouc-Wen model

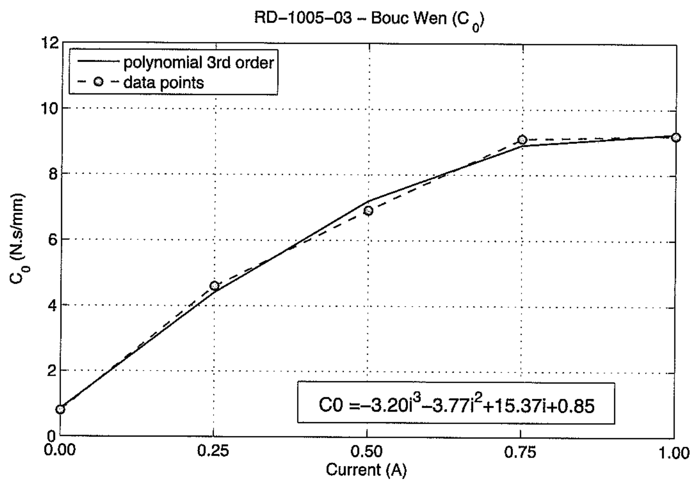

Figure 23: Curve fitting for $c_0(I)$ of the Bouc-Wen model

According to the curve fitting shown in Figure 22, the parameter α is described by

$$f_c(I) = -305.60I^3 + 377.83I^2 + 103.87I + 11.76 \text{ (N/mm)} \tag{15}$$

The same procedure was used for the model parameter c_0 and a third order function was selected and is given by

$$c_0(I) = -3.20I^3 - 3.77I^2 + 15.37I + 0.85 \text{ (N/mm)} \tag{16}$$

Results of experimental and numerical responses for 1.5Hz sinusoidal excitation, 4mm of amplitude and operating current of I= 1.00A are presented in Figure 24.

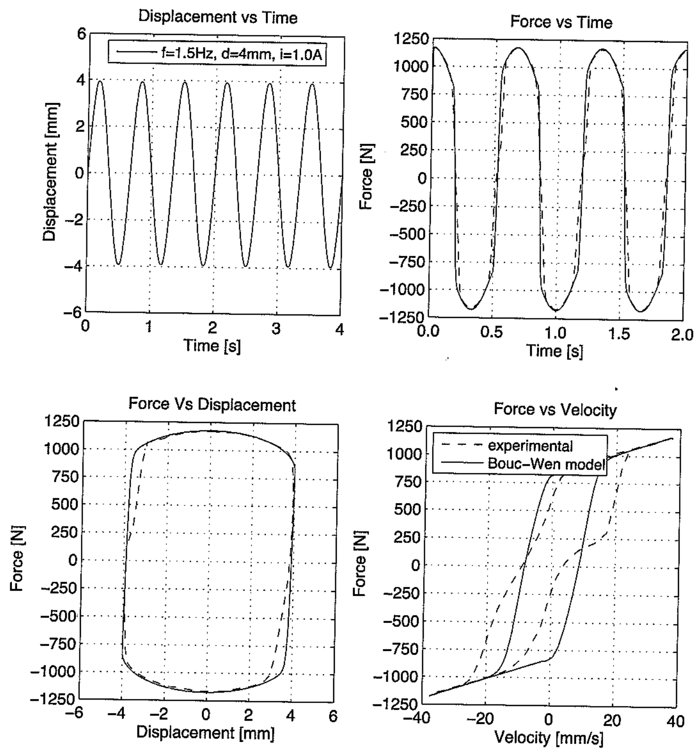

Figure 24: RD-1005-3 MR damper – Experimental vs. numerical response for the Bouc-Wen model (1.50 Hz sinusoidal excitation with 4mm amplitude and 1.00A)

The results show that the simple Bouc-Wen model is able to characterize the MR damper hysteretic response. However, the predicted computational results are still far from a perfect representation of the hysteretic behaviour.

This divergence is caused by the complexity of the MR fluid behaviour associated with the accumulator influence in the global MR damper response.

4.3 Modified Bouc-Wen model

The Modified Bouc-Wen model or Spencer model is a variation of the simple Bouc-Wen model presented previously. This model was developed to improve the nonlinear force-velocity hysteretic response of MR dampers since the simple Bouc-Wen model does not reflect the roll-off effect in the region where the acceleration and velocity have opposite signs and the magnitude of the velocities are small [7].

This model includes a simple Bouc-Wen block and two new mechanical components: a spring and a dashpot connected as shown in Figure 2. The spring represents the accumulator stiffness and is characterized by the model parameter k_1; while the dashpot, defined by the model parameter c_1, is included in the model to create the roll-off effect that is observed in the experimental data at low velocities. In this model, k_0 controls the stiffness at large velocities and x_0 represents the initial displacement of the spring k_1 (related to the force offset during the experimental tests as a result of the accumulator existence).

The effect of the model parameter c1 in the hysteretic loops is displayed in Figure 25. The numerical responses were made for a variable value of c_1 while the rest of the model parameters are kept to a constant value. This analysis shows that increasing the value of c_0 produces an increase in the hysteretic loop slope along with an increase in the hysteretic loop width. Moreover, the characteristic "S" shape of the hysteretic loop is visible for moderate or high values of c1 (for the present constant model parameters). In this case, the typical hysteretic loop is achieved when the value of c1 is significantly higher than the value of c_0 (c_1>10c_0).

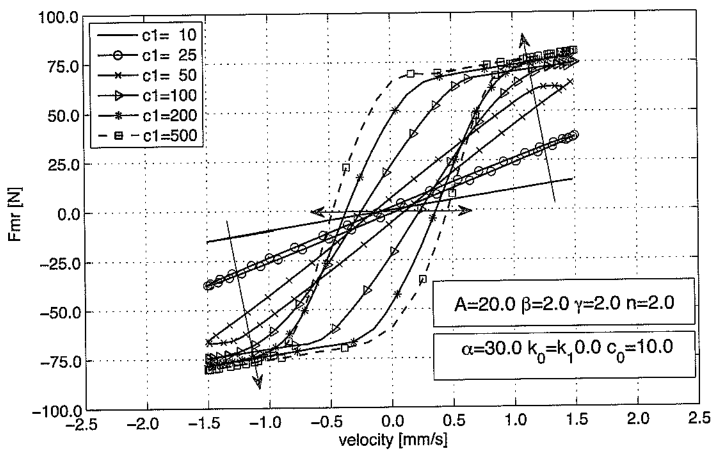

Figure 24: Influence of parameter c_1 on force-velocity curves

Although the overall effect of this parameter can be characterized by the curves plotted in Figure 25, is important to notice that the effect of this parameter is also dependent on the rest of the Bouc-Wen model parameters and different shapes can be obtained by changing the other parameters.

The roll-off effect observed in the experimental data at low velocities can be adjusted, varying this parameter in combination with the Bouc-Wen parameters.

Finally, the effect of the spring parameter k_1 is shown in Figure 26. This parameter has a similar effect as k_0, *i.e.*, increasing the value of k_1 produces a widening of the hysteretic loop.

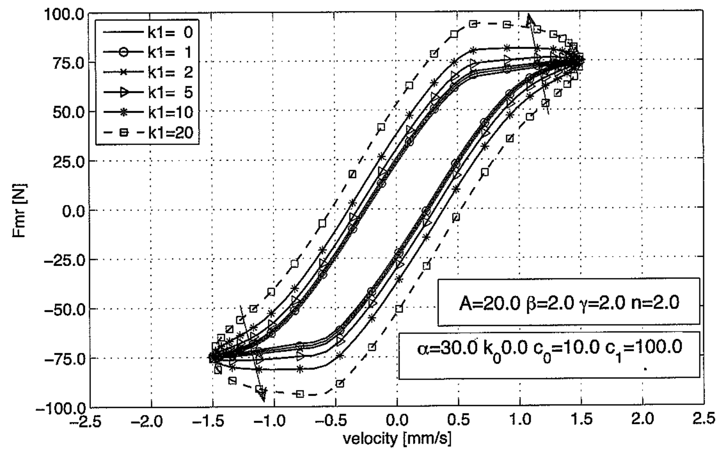

Figure 26: Influence of parameter k_1 on force-velocity curves

The experimental results obtained with these MR damper show that this widening effect is insignificant, which suggests that the contribution of the linear springs to the shape of the hysteretic loop is negligible compared to other model components.

The force generated by the MR damper is defined by the seven parameters of the Bouc-Wen block (A, β, γ, n, c_0, k_0, and α) and two new model parameters k_1 and c_1 related to the new mechanical components. Thus, the identification procedure involves nine model parameters (A, β, γ, α, c_0, k_0, k_1, c_1, and n), or ten if the force offset f_0 (or x_0) is considered as a variable to be identified, and the parameter vector is then defined as

$$\Theta = [\alpha, \beta, A, n, k_0, k_1, c_0, c_1, x_0] \qquad (17)$$

The effect of each parameter on the hysteretic loop shape was considered to define the necessary parameter constraints to enhance the identification procedure. The damper has a softening hysteretic effect with no signs of hardening (case I, II or III, *i.e.*, (β+γ) > 0) and the parameters A, α, k_0, and c_0 are positive variables. The parameter c_0 should have a reduced value to avoid steep slopes, and k_0 should be close to zero to reduce the widening effect. It was assumed that n=2 and the force offset, defined by $k_1(x-x_0)$ which represents the force as a result of the accumulator existence, and has the same value as the Bingham and the simple Bouc-Wen model force offset (f_0 =40 N). The parameter c_1 is much higher than c_0 (a constraint $c_1 > 5c_0$ was imposed in this study) and the spring parameter k_1 has a small value as a result of the reduced widening effect observed in the experimental data. The different hysteretic loops of the numerical model were determined by a set of model parameters for each experimental excitation case.

Figure 27 shows the result that was obtained with the parameter identification procedure for the Modified Bouc-Wen model (1.50 Hz, 4 mm and 0.75 A).

This procedure was repeated for each set of experimental data and the values of the model parameters of the Modified Bouc-Wen model were determined for each dataset.

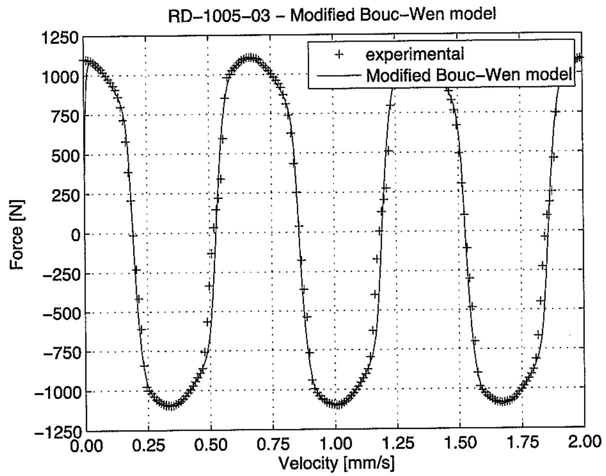

Figure 27: RD-1005-3 MR damper – Parameter identification of the Modified Bouc-Wen model (1.50 Hz, 4mm and 0.75A)

The average values of the current independent parameters A=10.013, β=3.044 mm^{-2}, γ=0.103 mm^{-2} and k_0 =1.121 N/mm were found. The parameters α, c_0, and c_1 are described as functions of the input current by a polynomial curve fitting procedure as shown in Figures 28-30.

According to the curve fitting procedure, the model parameters α, c_0, and c_1 can be described by

$$\alpha(I) = -826.67I^3 + 905.14I^2 + 412.52I + 38.24 \text{ (N/mm)} \quad (18)$$

$$c_0(I) = -11.73I^3 + 10.51I^2 + 11.02I + 0.59 \text{ (N/mm)} \quad (19)$$

$$c_1(I) = -54.40I^3 + 57.03I^2 + 64.57I + 4.73 \text{ (N/mm)} \quad (20)$$

Results of experimental and numerical responses of the MR damper are presented in Figure 31 (1.5 Hz, 4 mm of amplitude and I=1.00 A).

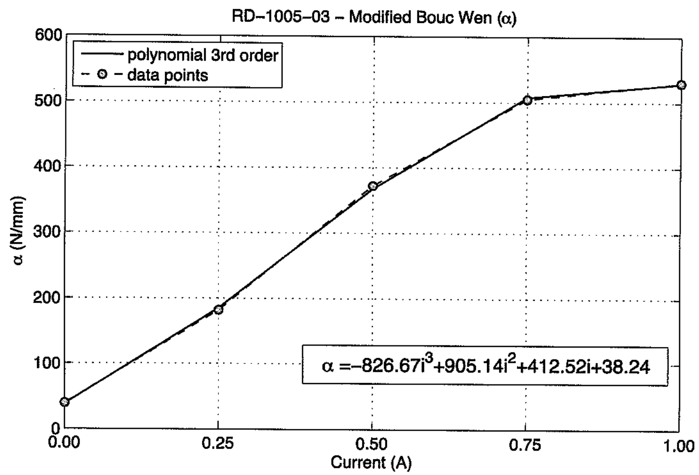

Figure 28: Curve fitting for $\alpha(I)$ of the Bouc-Wen model

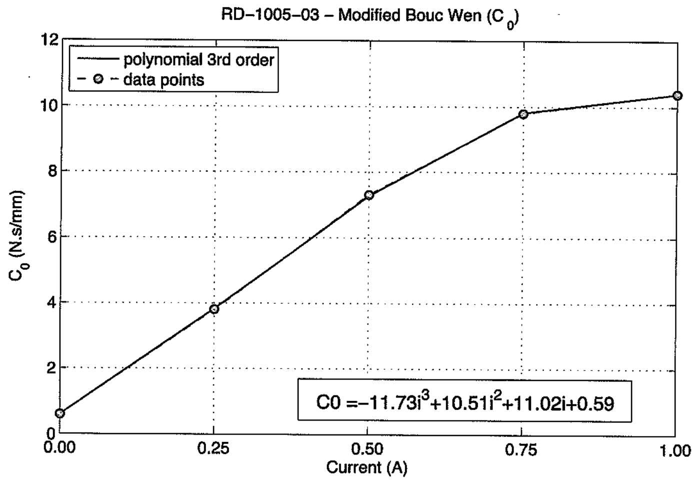

Figure 29: Curve fitting for $c_0(I)$ of the Bouc-Wen model

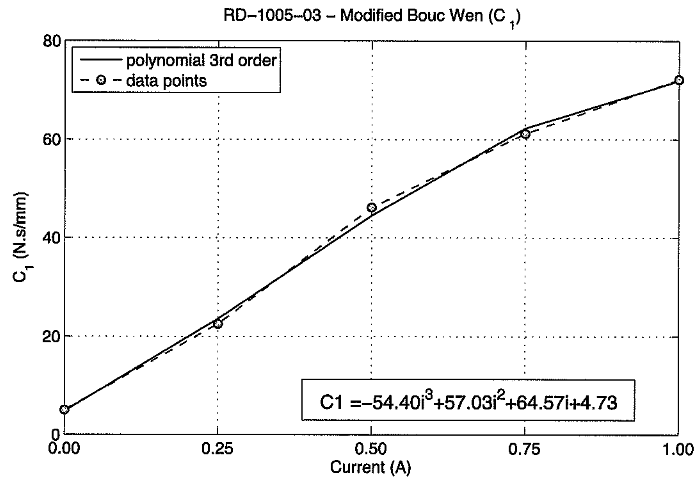

Figure 30: Curve fitting for $c_1(I)$ of the Bouc-Wen model

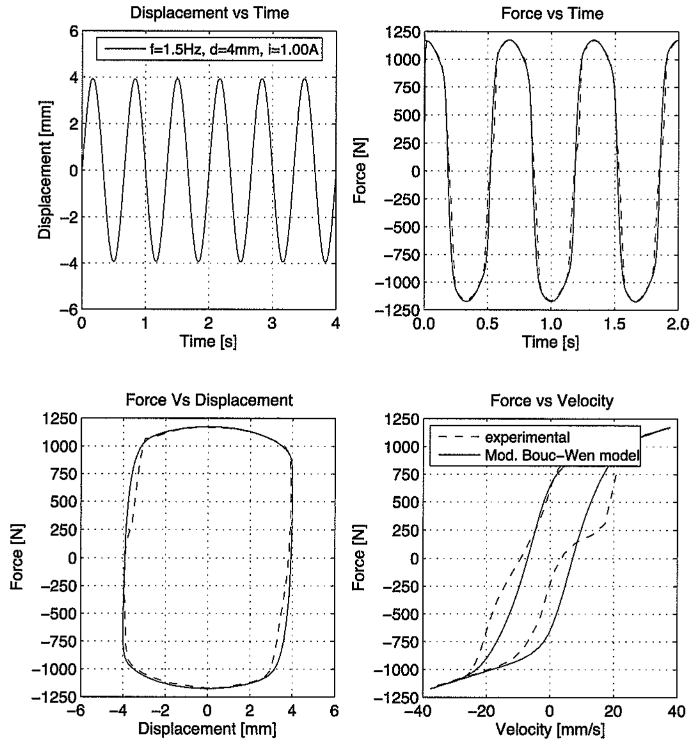

Figure 31: RD-1005-3 MR damper – Experimental vs. numerical response for the Bouc-Wen model (1.50 Hz sinusoidal excitation with 4mm amplitude and 1.00A)

The results show that the Bouc-Wen model is able to characterize the MR damper hysteretic response. However, as a consequence of the complexity of the MR fluid behaviour associated with the accumulator influence in the global MR damper response, the predicted computational results are still far from a perfect representation of the hysteretic behaviour. Nevertheless, they are considerably better than the ones obtained with the Bingham model, and improve the results of the simplified Bouc-Wen model.

In the previous analysis, three common parametric models were used to numerically simulate the response of the RD-1005-3 MR damper.

Figure 32 shows the numerical response of the Modified Bouc-Wen, the simple Bouc-Wen, and the Bingham models compared to the experimental data (1.50 Hz, 5 mm and 0.50 A). These models are possible modelling approaches with different levels of complexity and corresponding levels of accuracy.

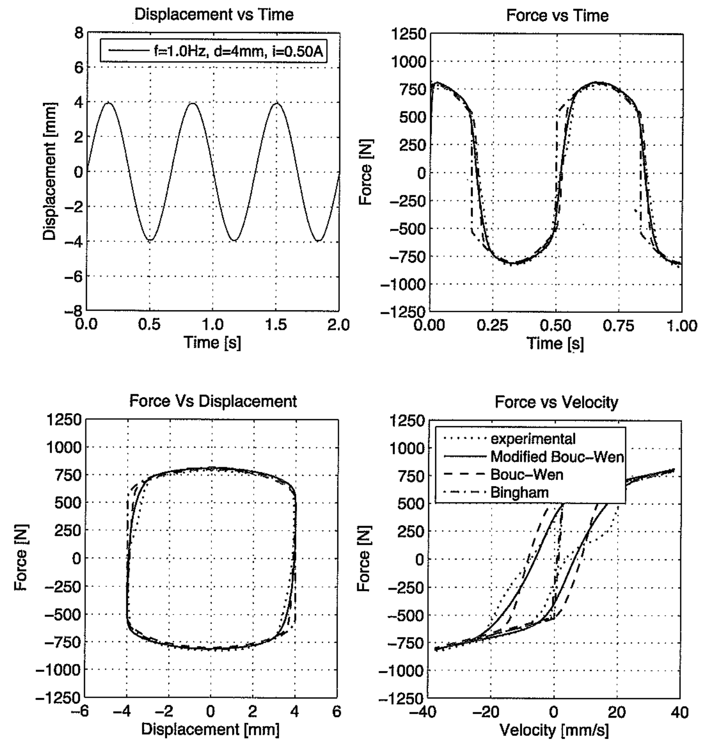

Figure 32: RD-1005-3 MR damper – Experimental vs. numerical response for the Modified Bouc-Wen, Bouc-Wen and Bingham models (1.50 Hz, 5mm and 0.50A)

This latter figure allows a comparison of the performance of the three parametric models and their ability to accurately predict the MR damper non-linear response under sinusoidal excitation.

The Bingham model can be used in very simple simulations of the damper response; although this model can reproduce the overall response, it is unable to process the typical non-linear hysteretic behaviour of these dampers. It can be verified that this model is able to represent the overall MR damper response by a simple mathematical function, but without the capacity to simulate its non-linear hysteretic behaviour, which can be a very detrimental limitation when a very accurate numerical response is needed.

The simple Bouc-Wen model is a more detailed model with the ability to simulate the non-linear hysteretic response; but the resulting hysteretic loops are incapable of reproducing the roll-off effect observed at low velocities.

To overcome this problem, the enhanced Modified Bouc-Wen was developed and the roll-off effect was introduced in the numerical simulation.

The drawback of the more elaborated modes is related to the number of parameters that are involved in the identification procedure, which increases the required computational work.

But this is completely justified by the importance of the structures to protect, that is, to which the structural dynamic control is applied through MR devices.

5 Conclusions

The present article addressed the non-linear hysteretic properties of MR dampers, presenting a general review of the available parametric modelling approaches. In the first section the properties of MR fluids were presented to introduce the rheological effect that constitutes the fundamental feature required to develop "smart" damper technology. Then, the parametric models were presented and three of the most common approaches were extensively reviewed. An experimental testing procedure was carried out to characterize the response of a commercial MR damper and the experimental data were used to develop several numerical models. These models require the definition of some model parameters that must be initially found to construct a realistic numerical response. Thus, an identification routine was developed and the predicted response was compared to the experimental data. As expected, more complex models are computationally cumbersome but are significantly more accurate than simpler models.

Acknowledgements

The authors gratefully acknowledge the funding by Ministério da Ciência, Tecnologia e Ensino Superior, FCT, Portugal, under grant SFRH/BD/49094/2008.

References

[1] J. Rabinow, "The magnetic fluid clutch". AIEE Trans., 67, 1308–1315, 1948.

[2] E. Guglielmino, T. Sireteanu, C.W. Stammers, G. Ghita, M. Giuclea, "Semi-active suspension control: improved vehicle ride and road friendliness", Springer, 2008.

[3] W. Wu, C. Cai, "Experimental Study of Magnetorheological Dampers and Application to Cable Vibration Control", Journal of Vibration and Control, 12-1, 67-82, 2006.

[4] G. Serino, A. Occhiuzzi, "A Semi-Active Oleodynamic Damper for Earthquake Control. Part 2: Evaluation of Performance Through Shaking Table Tests", Bulletin of Earthquake Engineering, 1, 269-301, 2003.

[5] W.H. Li, G.Z. Yao, G. Chen, S.H. Yeo, F.F. Yap, "Testing and steady state modeling of a linear MR damper under sinusoidal loading", Smart Materials and Structures, 9, 95-102, 2000.

[6] B. Sapiński, J. Filuś, "Analysis of parametric models of MR linear damper", Journal of Theoretical and Applied Mechanics, 41(2), 215-240, 2003.

[7] J.M. Ginder, "Rheology Controlled by Magnetic Fields", Encyclopedia of Applied Physics, 16, 487, 1996.

[8] M. Braz-Cesar, R. Barros, "Semi-Active Control of an Experimental Frame using MR Dampers: numerical results and experimental validation", COMPDYN 2011 – 3rd International Conference on Computational Methods in Structural Dynamics & Earthquake Engineering, 2011.

[9] M.B. Cesar, R.C. Barros, "Semi-Active Vibration Control of a Three Degree-of-Freedom Scaled Frame with a Magneto-Rheological Damper", in B.H.V. Topping, J.M. Adam, F.J. Pallarés, R. Bru, M.L. Romero, (Editors), "Proceedings of the Tenth International Conference on Computational Structures Technology", Civil-Comp Press, Stirlingshire, UK, Paper 169, 2010. doi:10.4203/ccp.93.169

[10] M. Braz-César, R. Barros, "Semi-active Vibration Control of Buildings using MR Dampers: Numerical and Experimental Verification", 14th ECEE – 14th European Conference on Earthquake Engineering, 2010.

[11] M. Braz-César, R. Barros, "Properties and Numerical Modeling of MR Dampers", 15th ICEM - 15th International Conference on Experimental Mechanics, Porto, 2012 (in press).

[12] D.H. Wang, W.H. Liao, "Magnetorheological fluid dampers: a review of parametric modelling", Smart Materials and Structures, 20, 023001, 2011.

[13] F. Gandhi, W. Bullough, "On the Phenomenological Modeling of Electrorheological and Magnetorheological Fluid Preyield Behavior", Journal of Intelligent Material Systems and Structures, 16(3), 237-248, 2005.

[14] F. Goncalves, J. Koo, M. Ahmadian, "A Review of the State of the Art in Magnetorheological Fluid Technologies – Part I: MR Fluid and MR Fluid Models", The Shock and Vibration Digest, 38(3), 203-219, 2006.

[15] S. Guo, S. Yang, C. Pan, "Dynamic Modeling of Magnetorheological Damper Behaviors", JIMSS, 17(1), 3-14, 2006.

[16] M. Maślanka, B. Sapiński, "Experimental Study of Vibration Control of a Cable with an Attached MR Damper", Journal of Theoretical and Applied Mechanics, 45(4), 893-917, 2007.
[17] B.F. Spencer Jr., S.J. Dyke, M.K. Sain, J.D. Carlson, "Phenomenological model of a magnetorheological damper", Journal of Engineering Mechanics, 123, 230-238, 1997.
[18] M.T. Avraam, "MR-fluid brake design and its application to a portable muscular rehabilitation device", PhD thesis, 2009.
[19] M. Kamath, H. Hurt, N. Wereley, "Analysis and Testing of Bingham Plastic Behavior in Semi-Active Electrorheological Fluid Dampers", Smart Material & Structures, 5, 576–590, 1996.
[20] Y.K. Wen, "Method for random vibration of hysteretic systems", Journal of the Engineering Mechanics Division, 102(2), 249-263, 1976.
[21] W. Schwanen, "Modelling and identification of the dynamic behavior of a wire rope spring", Masters thesis, 2004.
[22] C.W. Wong, Y.Q. Ni, J.M. Ko, "Steady-State oscilliation of hystereric differential model. I: Response analysis", Journal of engineering mechanics, 120, 2271-2298, 1994.
[23] F. Ikhouane, J. Rodellar, "Systems with hysteresis: Analysis, identification and control using the Bouc-Wen model", John Wiley & Sons, 2007.
[24] The Mathworks, Inc. "Optimization Toolbox User's Guide", USA, 2012.